Shape Analysis of Corpus Callosum in Phenylketonuria Using a New 3D Correspondence Algorithm

Qing He[*1], Shawn E. Christ[2], Kevin Karsch[1], Dawn Peck[3], Ye Duan[1]

[1] Department of Computer Science, University of Missouri, Columbia, MO, USA 65211
[2] Department of Psychological Sciences, University of Missouri, Columbia, MO, USA 65211
[3] Department of Child Health, University of Missouri, Columbia, MO, USA 65211

ABSTRACT

Statistical shape analysis of brain structures has gained increasing interest from neuroimaging community because it can precisely locate shape differences between healthy and pathological structures. The most difficult and crucial problem is establishing shape correspondence among individual 3D shapes. This paper proposes a new algorithm for 3D shape correspondence. A set of landmarks are sampled on a template shape, and initial correspondence is established between the template and the target shape based on the similarity of locations and normal directions. The landmarks on the target are then refined by iterative thin plate spline. The algorithm is simple and fast, and no spherical mapping is needed. We apply our method to the statistical shape analysis of the corpus callosum (CC) in phenylketonuria (PKU), and significant local shape differences between the patients and the controls are found in the most anterior and posterior aspects of the corpus callosum.

Keywords: 3D shape correspondence, statistical shape analysis, thin plate spline, corpus callosum, phenylketonuria

1. INTRODUCTION

Quantitative morphologic assessment of individual brain structures is often based on volumetric measurements and shape analysis. Volume changes are intuitive features in explaining atrophy or dilation due to illness. However, shape analysis can precisely locate morphological changes in pathological structures which cannot be reflected in volume measurements, thus shape analysis has gained increasing interest from the neuroimaging community.

The main challenge in shape analysis is the required step of establishing shape correspondence among individual shapes. In this way, each shape instance is represented by a certain number of corresponded landmark points, which facilitate the statistical comparison of shapes between different groups. Note that the corresponded landmarks are not necessarily coincident with anatomically significant points of a structure [1]. There are usually only a small number of anatomically meaningful points on a structure, while the corresponded landmarks on a shape should be dense enough to accurately represent the shape. Shape correspondence is a difficult problem especially in 3D case, because of the non-linear shape description and non-rigid shape variation. Prior research [2,3] reveals that a small error in shape correspondence may substantially influence the accuracy of the statistical shape analysis.

Many methods have been developed for shape correspondence in recent years [1-7]. They can be classified into two types: mapping based and non-mapping based. Mapping based methods need to first map each shape instance onto a sphere (or ellipsoid), such as minimum description length (MDL) [3,4] and spherical harmonics descriptors (SPHARM) [5,6]. In MDL, the shape correspondence error is measured by the required bit-length to transmit the resulting statistical shape model and all the training shape instances. SPHARM use first order ellipsoid from the spherical harmonic coefficients to align the spherical parameterization through which the correspondence among 3D shape instances is established. The spherical mapping of the shape instance is computationally expensive. Moreover, this type of methods is not appropriate for non-sphere-like shapes because of the extreme distortion in the mapping.

Non-mapping based approaches do not require any spherical mapping of the shape surface so that the complexity is greatly reduced, such as shape context [7-10] and landmark sliding [1]. Shape context was first proposed in [7] for 2D shape matching and it has been extended to 3D shapes later [9,10]. The definition of shape context is a local histogram of edge points in a radius-angle grid [7]. Given a set of points on the template shape, we find the matching points on the target shape whose shape contexts are similar to the points on the template. Note that this matching may not be complete, i.e., only part of the target points are matched to part (or all) of the template points, and the unmatched points on both shapes are dummy points. A transformation from the target to the template is then

[*] qhgb2@mizzou.edu; phone: 1 573 882 3951

estimated by thin-plate spline (TPS) [18], and the point correspondence is estimated again between the template and the transformed target shape. After several iterations the matching result will be significantly improved. However, there may still be dummy points on the template or target shape at the convergence of the iteration. This may cause a problem in the correspondence among more than two shapes because the number of matched points is not fixed between each pair of shapes. Landmark sliding algorithm can achieve correspondence among a group of 3D shapes with less computational cost and the result is comparable to those of MDL and SPHARM. It first constructs an initial correspondence between two shapes after rigid alignment, and then refines the matched points on the target shape by sliding the points along the tangent direction. The sliding criterion is to minimize a shape correspondence error defined by TPS energy. This algorithm can be easily generalized to more than two shapes as long as we keep the template shape fixed.

In this paper, we develop a non-mapping based method for 3D shape correspondence. Our method is similar to the landmark sliding algorithm in [1], but there are two main differences. First, the initial correspondence algorithm in [1] is not robust for all kinds of shapes. We improve this algorithm by adding surface normal constraints so that it can overcome the problem in the corpus callosum shape. This problem will be shown later in the paper, and it is very common in non-spherical shapes. Second, we do not use landmark sliding to refine the matched points. Instead, we perform iterative transformation and matching as in [7]. In this way, the matched points are faithful to the shape because they are original surface points. It can also prevent some points from sliding too far away from the surface. We apply our method to the statistical shape analysis of the corpus callosum in individuals with early-treated phenylketonuria (PKU), a genetic condition associated with white matter and corpus callosum abnormalities [15-17, 19, 26]. To anticipate the results, a significant local shape difference between PKU patients and the controls was found.

The next section presents our method in detail, and section 3 shows the results in the shape analysis of the corpus callosum. Section 4 concludes the paper with some discussion.

2. METHODS FOR 3D SHAPE CORRESPONDENCE

In this section we consider the correspondence between two 3D shapes. The input is two triangle meshes, the template U and the target V. For the correspondence among a group of shapes, we can randomly choose one as the template, and correspond each of the other shapes to this template using the same method.

2.1 Spatial alignment and landmark sampling on the template

The first two steps are very similar to those in [1], and we only give a brief description here. The algorithm begins with a spatial alignment. Given two triangle meshes U and V, we first remove the location difference by moving their centers of mass to the origin. Then we normalize each shape by their centroid size [18] so that there is no size effect in the following shape analysis. The rotation between the two shapes is removed by aligning their principle axes. The details of the rotation alignment can be found in [1].

After alignment we construct a set of landmarks on the template shape U. These landmarks need not to be anatomically defined. The basic consideration is that they should be dense enough to represent the surface U and sufficiently sparse for a compact statistical shape model [1]. The 3D space is divided into equal-sized cubic cells. In each cell, the surface point closest to the center of the cell is selected as the landmark [1]. The size of the cell controls the density of landmarks. Typically, there are thousands of points on a 3D mesh, but the computational cost will be expensive if we include all points in the shape analysis. Only a few hundred of landmarks are sampled and used for shape analysis purpose. A comparison of the original surface points and the sampled landmarks can be seen from Fig.2(a) and (c).

2.2 Initial correspondence on the target shape

The initial correspondences on the target V is constructed in a simple way [1]. Specifically, for each landmark on the template, a point on the target triangle mesh which is closest to this landmark is selected as the target landmark. Since the two shapes are pre-aligned, it is assumed that this simple method can find a rough correspondence between the landmarks on U and V [1]. Generally, this simple method can work well for many types of shapes. However, if the two aligned shapes do not have a certain amount of overlapping, this method may fail to find the correct correspondence. The following example of the corpus callosum shape will illustrate this problem. Fig. 1 shows two corpus callosum shapes after spatial alignment. For simplicity, only 2D shapes are shown and the 3D case is similar. The major parts of the bodies of the two shapes do not overlap. For point A on the template (Fig.1), its closest match on the target shape is point A', but obviously this correspondence is not correct because A is on the lower body of the corpus callosum and A' is on the upper body. In this case, it will be very difficult to correct it in the following landmark refining. This problem is very common since there is large variation among corpus callosum shapes.

In order to solve this problem, we propose an improved initial correspondence algorithm with a mutual selection strategy and normal constraints. We observe that if the two points are corresponded points on two shapes, their surface normal directions should not differ too much. If their surface normal directions are nearly opposite (e.g, A and A' in Fig. 1), they are not likely to be the corresponded points. We use the constraint of normal directions in addition to the distance in the landmark selection procedure. Let the set of template landmarks obtained in 2.1 be U_L, each template landmark $u_i \in U_L$, the original point set on the target mesh be V, each target point $v_i \in V$, and the set of target landmarks be V_L. Our algorithm can be outlined as follows.

1. For each $v_j \in V$, find a landmark u_i from U_L which is closest to v_i. Usually many target points will find the same template landmark u_i because the points in V are much denser than in U_L.

2. For each $u_i \in U_L$, record all the v_j's that select u_i as the closest point. Denote this set of v_j's as V_i. The points in V_i are the candidate points to match the landmark u_i.

3. If u_i has more than one point in its V_i, find a point v_j from V_i whose normal direction is closest to the normal of u_i. Remove v_j from V and add it to V_L. If u_i has no points in its V_i, find a point v_j from V that has closest distance to u_i. Remove v_j from V and add it to V_L.

The resulting points in V_L are the corresponding landmarks on the target shape. The index of each point in V_L is the same as the index of its matched point in U_L, so the correspondence between U_L and V_L is established. Fig.1 again illustrates how our algorithm overcomes the aforementioned problem. Target points A' and B both select A as the closest point in step 1, but A selects B as its correspondence because the normal directions of B and A are close. No target point selects C in step1, so C selects a closest point as its correspondence which is A' in step 3. Fig.2 shows a real example of the initial landmarks on the target corpus callosum shape obtained using the algorithm in [1] and our algorithm respectively. Sagittal view of the 3D model is displayed. Two aligned original shapes are shown in Fig.2(a) which is similar to the case in Fig.1. Only point clouds are shown here without triangle meshes. The upper body of the target shape is missing in the result of the algorithm in [1] (Fig.2(b)). The landmarks in our results, however, can correctly represent the target shape (Fig.2(c)).

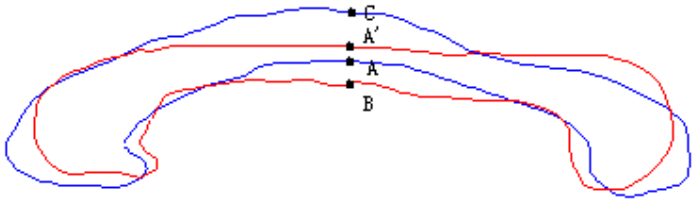

Fig.1 Illustration of the case where the algorithm in [1] will fail. (blue: template; red: target)

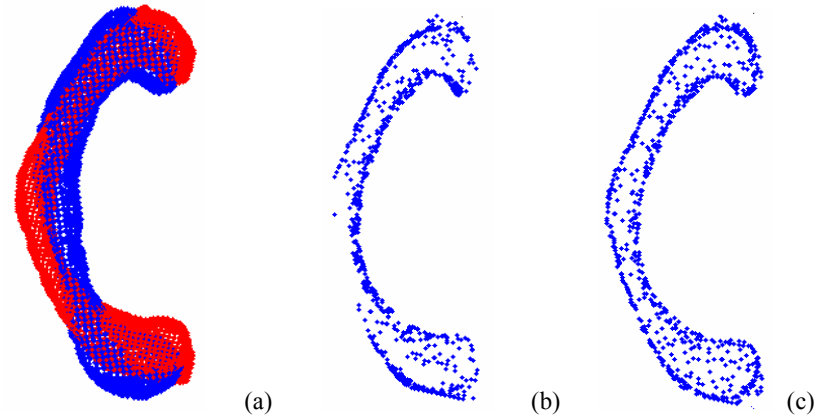

Fig. 2 (a) two aligned original point clouds overlaid (blue: template, red: target) (b) initial landmarks on the target shape obtained using the algorithm in [1] and (c) our algorithm

2.3 Refining landmarks by iterative TPS

Given the initial correspondence between two sets of landmarks, U_L and V_L, one can estimate a transformation T from V_L to U_L, and T can be applied to the entire target point set V. In [7], TPS transformation is used iteratively to refine the shape context matching. Similarly, we can perform our algorithm in 2.2 and TPS transformation iteratively to refine the shape correspondence. We will now briefly introduce the basic concept of TPS. Suppose there are n

landmarks in U_L and V_L respectively. Let the landmarks in U_L be $u_i = (u_{ix}, u_{iy}, u_{iz})$, and the landmarks in V_L be $v_i = (v_{ix}, v_{iy}, v_{iz})$, *i=1...n*. u_i and v_i are corresponded points for the same *i*. The TPS function which transforms v_i to u_i has the form:

$$f(v_{ix}, v_{iy}, v_{iz}) = a_0 + a_x v_{ix} + a_y v_{iy} + a_z v_{iz} + \sum_{j=1}^{n} w_j \phi(\| (v_{jx}, v_{jy}, v_{jz}) - (v_{ix}, v_{iy}, v_{iz}) \|) \quad (1)$$

where $\phi(r) = r$ in 3D case. We use three separate functions to model the transformation of x,y,z coordinates, and the objective function is

$$T(v_{ix}, v_{iy}, v_{iz}) = (f_x(v_{ix}, v_{iy}, v_{iz}), f_y(v_{ix}, v_{iy}, v_{iz}), f_z(v_{ix}, v_{iy}, v_{iz})) = (u_{ix}, u_{iy}, u_{iz}) \quad (2)$$

Each function *fx, fy,fz* has the same form as (1). Equation (2) can be written in the matrix form and the coefficients a_0, a_x, a_y, a_z, w_i of each function can be solved from the linear equation.

After we obtain the initial correspondence between U_L and V_L, we estimate a TPS transformation from V_L to U_L, and apply the transformation function to the entire point set V. The transformed target point set is denoted as V^1, and the algorithm in 2.2 is then applied on U_L and V^1 to find a set of target landmarks $V^1{}_L$. Then a TPS transformation from $V^1{}_L$ to U_L is estimated and applied to V^1. The final landmark set $V^n{}_L$ after *n* iterations contains the landmarks in the transformed shape V^n. We keep track of the indices of the landmarks in each iteration, so that the final landmarks can be easily mapped to their original coordinates in V. After several iterations, the initial correspondence error can be greatly reduced. As suggested in [7], three iterations are used in our experiment. Fig.3 shows one example of landmarks before and after three TPS iterations.

While the landmark sliding in [1] can obtain similar results of refined landmarks, our method requires less computational time, and all the sampled landmarks are on the original surface without sliding away.

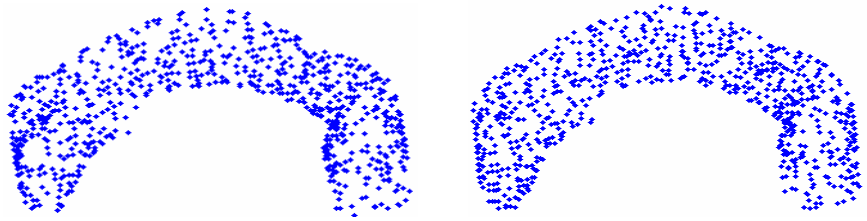

Fig.3 The landmarks on a target shape before (left) and after (right) TPS iterations

3. STATISTICAL SHAPE ANALYSIS

We apply our shape correspondence algorithm to the shape analysis of the corpus callosum in PKU. PKU is a metabolic disorder resulting from a deficiency of phenylalanine hydroxylase, which leads to elevated levels of the amino acid phenylalanine (Phe) in the blood. It is an autosomal recessive disorder caused by mutations in the PAH gene. The clinical behavior of untreated state is characterized by mental retardation, macrocephaly, seizures, eczema, and other behavior abnormalities [21], and the brain pathology includes reduced brain weight and hypo- and demyelination of cerebral white matter [22]. However, the heterogeneity in the mutations of PAH results in wide phenotypic heterogeneity, and the relationship between the clinical phenotype and the genotype is not always constant [21].

From a neurological standpoint, PKU, both treated and untreated, is associated with white matter injury [15-17]. The corpus callosum is a large white matter bundle connecting the left and right hemisphere and is the main neural conduit for interhemispheric interaction. Studies have found that patients with early-treated PKU displayed a disruption in communication between hemispheres, consistent with abnormal myelination of neurons that make up the corpus callosum [23,24]. Additional evidence for CC irregularities in PKU comes from recent findings of decreased volume [17, 19] and disrupted microstructural integrity [26] in CC of individuals with early-treated PKU as compared to non-PKU controls. However, no shape analysis of the CC has been done in regard to PKU.

Eight participants with PKU (4 males, 4 females) who were diagnosed at birth and maintained on a phenylalanine-restricted diet participated in the study and ranged in age from 11 to 27 years (M = 16.80, SD = 4.92). Eight individuals without PKU (4 males, 4 females) comprised an age-, education-, and gender-matched control group.

The control group ranged in age from 12 to 27 years (M = 17.19, SD = 5.05). Individuals with psychiatric and/or medical history unrelated to PKU were excluded.

All MRI scans were obtained on a 1.5T Siemens Symphony scanner with a standard 8-channel head coil. A high-resolution three-dimensional T1-weighted sagittal scan was collected for purposes of structural analysis (MP-RAGE sequence: TR = 1920 ms, TE = 4 ms, flip angle = 8°, in-plane resolution = 1 x 1 mm, slice thickness = 1 mm, number of slices = 160).

The CC models were obtained using a 3D semi-automatic hybrid (region- and boundary-based) segmentation method that had been previously validated for accuracy and reproducibility [20]. To increase the accuracy and validity of the results, we ensured that all segmentations were completed by the same trained individual. Each model was a 3D mesh with 3000~4000 points.

One of the 16 meshes was randomly selected as the template, and 767 landmarks were sampled on this template. The correspondence between this template and each of the other shapes was established using our algorithm, and the result was 16 sets of corresponded landmarks, which can be used directly for statistical shape analysis. The experiment was running on an Intel(R) Pentium(R) D (2.8GHz) PC with Windows Vista, and all the codes were written in Matlab. The average time to process one target shape was about 2 minutes.

Since each shape is spatially aligned with the template before the shape correspondence is established, no additional spatial alignment is necessary among all the shapes. The difference in the size of the CC has been eliminated in the spatial alignment, so the shape analysis only reveals pure shape difference between patients and controls. Hotelling T^2 two-sample metric is used to measure how two groups of shapes are different from each other at each surface location. We use a modified T^2 metric instead of the standard one, because it is less sensitive to group differences of the covariance matrixes and the sample size [5]. This metric is defined as

$$T^2 = (\mu_1 - \mu_2)'((1/n_1)\Sigma_1 + (1/n_2)\Sigma_2))^{-1}(\mu_1 - \mu_2) \qquad (3)$$

where Σ_1, Σ_2 are the covariance matrixes of the two groups, μ_1, μ_2 are the average coordinates of the two groups at this surface point, and n_1, n_2 are the sample sizes of the two groups. A positive, larger T^2 indicates more significant group difference, and each T^2 is converted to a corresponding p-value at every surface location. This raw p-value is an optimistic estimation. Since comparisons are made at thousands of CC surface points, it is important to control for the multiple testing problem. There are several methods to deal with multiple comparison, such as random field [12,13], non-parametric permutation test [11] and false discovery rate estimation (FDR) [6]. In our work, we adopt FDR as the appropriate approach for p-value correction, because it provides an interpretable and adaptive criterion, while non-parametric permutation tests are overly pessimistic [5]. FDR method allows the false positive to be within a small proportion α (α =0.01 in our experiment). The p-value correction is computed as follows [6].

1. Sort the p-values such that $p_1 < p_2 < ... < p_N$, where N is the number of vertices on the surface.
2. From all the p-values that satisfy $p_i <= \alpha \bullet i/N$, select the p-value with the largest index i, denoted as p_α.
3. Declare all locations with p-values less than p_α significant.

Fig.4 gives a descriptive visualization of the group shape difference. Fig.4(a) shows the overlaid average shape of each group, and Fig.4(b) shows the signed distance map between the two average shapes rendered on an overall average shape of all 16 subjects. By examining the average structures, we find that in the patients the body of the CC is less bent, the anterior tip (genu) and posterior tip (splenium) are shorter, and the anterior most is more projected. Note that the triangle mesh information is lost after landmark sampling, and we reconstruct the surface from the landmarks using COCONE [14] for display purpose.

The significance maps of the raw and corrected p-values are shown in Fig.5. Smaller p-values indicate larger statistical significance. A two-tailed alpha level of 0.05 is chosen as the significance threshold for the raw p-values, and FDR threshold p_α is 0.01 for corrected p-values. Fig.5(a) shows the significance map of raw p-values, which is an optimistic estimation. The significance map of the corrected p-values (Fig.5(b)) shows that the major significant difference lies in the genu and splenium. This is consistent with the distance map in Fig.4(b) which shows the main difference between the averages at the these parts.

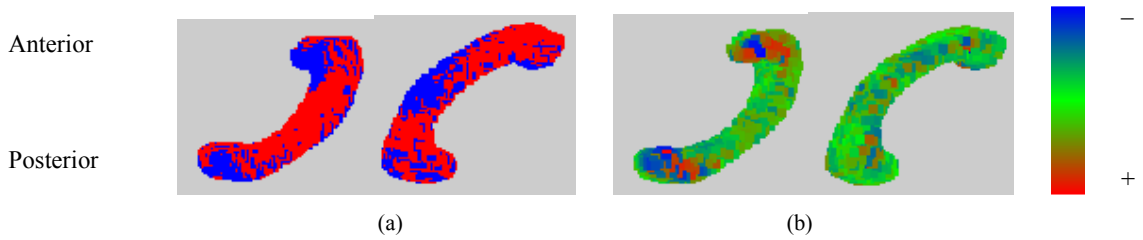

Fig.4. (a) Two views of the overlaid average shapes (blue: controls, red: patients) (b) Two views of the distance map between the two average shapes (The negative distances indicate the patients' structure is inside the controls' and the reverse is for the positive distances)

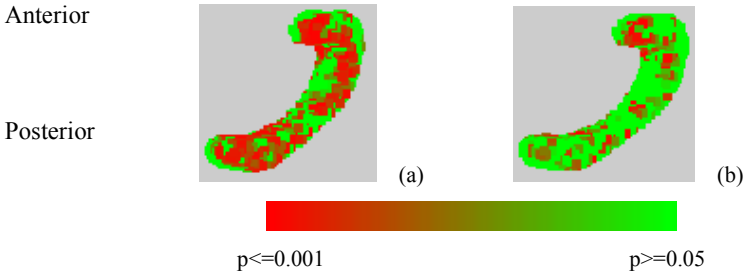

Fig.5. Significance map: (a) raw p values (b) corrected p values

4. DISCUSSION AND CONCLUSION

This paper presents a non-mapping based algorithm for 3D shape correspondence and applies it to the shape analysis of the corpus callosum in early-treated PKU. The correspondence is established among landmarks sampled from each individual shape. A set of landmarks dense enough to represent the surface are sampled on a template shape, and initial correspondence is established by finding matched landmarks on the target shape. A surface normal constraint in landmark selection is added in order to prevent mismatching. The landmarks on the target shape are then refined by iteratively applying TPS and the initial correspondence algorithm. All landmarks are faithful to the original surface since no landmark sliding is performed. Compared with mapping based methods, the implementation of our method is simple and fast.

There are two issues to be considered regarding our shape correspondence method. First, the landmark sampling on the template shape is arbitrary, and it will determine the point distribution on the rest of the shapes. It is not certain whether the discretization error in this sampling will affect the result of the shape analysis. Further experiment needs to be done to evaluate the influence of the sampling. Secondly, note that the landmarks in this paper are not real anatomical landmarks. Our landmarks are just a subset of surface points, while anatomical landmarks usually have biological meanings or geometrical prominence. Anatomical landmarks can usually be found consistently on different individual shapes; hence, locating anatomical landmarks may facilitate the correspondence establishment of the other surface points. Moreover, the exact matching of anatomical landmarks among individual shapes is crucial in clinical applications, but our current method cannot guarantee this exact matching. In the future, we plan to incorporate the correspondence of anatomical landmarks into our point correspondence establishment.

The statistical shape analysis revealed significant abnormalities in the genu and splenium of the CC in patients with PKU. This was true even though (1) all of the patients in the present study had received early and continuous dietary treatment and (2) clinical examination of the MRIs did not reveal any CC white matter hyperintensities. Taken together with previous studies [15-17, 19, 26], the current findings support the hypothesis that, whereas individuals with early-treated PKU are spared the severe neurological consequences associated with untreated PKU, they continue to experience detectable (albeit subtle) white matter abnormalities. Irregularities in the CC may contribute to the cognitive difficulties experienced by individuals with early-treated PKU. Indeed, early-treated PKU is associated with impairments in higher-order cognitive abilities (i.e., executive function) that require the integration of information across a wide variety of sources and thus rely heavily on the brain's white matter interconnections [25].

Although comparable with other preliminary studies utilizing MRI, the sizes of the clinical and comparison groups in the current investigation were small. Future studies utilizing a larger sample size would allow for the exploration of the potential relationship between CC shape and dietary control (as reflected by blood phenylalanine levels), age, cognitive profile, and other important factors. In the near future, we also hope to extend this line of research by

comparing measures of CC shape, microstructural integrity (as evaluated using diffusion tensor imaging), and function (as evaluated using functional MRI) within a single group of PKU participants.

ACKNOWLEDGEMENTS

This work is supported in part by a NIH pre-doctoral training grant for Clinical Biodetectives (M.M), Department of Defense Autism Concept Award (Y.D.), NARSAD Foundation Young Investigator Award (Y.D.), and University of Missouri Thompson Center Research Scholar Grant (S.E.C.).

REFERENCES

[1] Dalal P., Munsell B.C., Wang S., Tang J., Kenton O., Ninomiya H., Zhou X., Fujita H., "A Fast 3D Correspondence Method for Statistical Shape Modeling", IEEE Conference on Computer Vision and Pattern Recognition, Minneapolis, MN (2007)

[2] Bookstein F., "Landmark methods for forms without landmarks: Morphometrics of group differences in outline shape", Medical Image Analysis, 1(3):225-243 (1997)

[3] Davies R., Twining C., Cootes T., Waterton J., Taylor C., "A minimum description length approach to statistical shape modeling", IEEE Transactions on Medical Imaging, 21(5):525-537 (2002)

[4] Davies R.H., Twining C., Cootes T.F., Waterton J.C., Taylor C.J., "3D statistical shape models using direct optimisation of description length", 7th European Conference on Computer Vision, 3:3-20 (2002)

[5] Brechbuhler C., Gerig G., Kubler O, "Parameterization of closed surfaces for 3-D shape description", Computer Vision, Graphics and Image processing. 61:154-170, Springer (1995)

[6] Styner M., Oguz L., Xu S., Brechbuehler C., Pantazis D., Levitt J.J., Shenton M.E., and Gerig G, "Framework for the Statistical Shape Analysis of Brain Structures using SPHARM-PDM", ISC/NA-MIC Workshop on Open Science at MICCAI (2006)

[7] Belongie S., Malik J., Puzicha, J, "Shape matching and object recognition using shape contexts", IEEE Transactions on Pattern Analysis and Machine Intelligence**,** 24(4):509-522 (2002)

[8] Thayananthan A., Stenger B., Torr P.H.S., Cipolla R, "Shape context and chamfer matching in cluttered scenes", IEEE Conference on Computer Vision and Pattern Recognition, 1:127-133 (2003)

[9] Frome A., Huber D., Kolluri R., Buelow T., Malik J, "Recognizing objects in range data using regional point descriptors", 7th European Conference on Computer Vision, 224-237, Springer (2004)

[10] Kortgen M., Park G.J., Novotni M., Klein R, "3D shape matching with 3D shape contexts", 7th Central European Seminar on Computer Graphics (2003)

[11] Pantazis D., Leahy R.M., Nichol T.E., and Styner M, "Statistical surface-based morphometry using a non-parametric approach. Int. Symposium on Biomedical Imaging", 1283-1286 (2004)

[12] Chung M.K, Statistical Morphometry in Neuroanatomy, Ph.D. thesis, McGill University (2001)

[13] Worsley K.J., Marrett S., Neelin P., Vandal A.C., Friston K.J., Evans A.C, "A unified statistical approach for determining significant signals in images of cerebral activation. Human Brain Mapping", (4)58–73 (1996)

[14] Dey T. and Giesen J, "Detecting undersampling in surface reconstruction", Proc. 17th ACM Sympos. Comput. Geom., 257-263 (2001)

[15] Micheal D. Phillipsa, Peter McGrawa, Mark J. Lowea, Vincent P. Mathewsa and Bryan E. Hainlinea, "Diffusion-Weighted Imaging of White Matter Abnormalities in Patients with Phenylketonuria", American Journal of Neuroradiology 22:1583-1586 (2001)

[16] Hasselbalch S., Knudsen G.M., Toft P.B., et al, „Cerebral glucose metabolism is decreased in white matter changes in patients with phenylketonuria", Pediatr Res, 40:21-24 (1996)

[17] Pfaendner N.H., Reuner G., Pietz J., Jost G., Rating D., Magnotta V.A., Mohr A., Kress B., Sartor K., Hahnel S, "MR imaging-based volumetry in patients with early-treated phenylketonuria", American journal of neuroradiology, 2005, 26(7):1681-1685 (2005)

[18] Bookstein F, "Principal warps: Thin-plate splines and the decomposition of deformations", IEEE Transactions on Pattern Analysis and Machine Intelligence, 11(6):567-585 (1989)

[19] Hahnel S, "Brain MRI abnormalities in Phenylketonuria", Clinical Neuroradiology, 18:19-24 (2008)

[20] Karsch K., He Q., Duan Y., "A Fast, Semi-Automatic Brain Structure Segmentation Algorithm for Magnetic Resonance Imaging", IEEE International Conference on Bioinformatics and Biomedicine (2009)

[21] National Institutes of Health Consensus Development Panel, "National Institutes of Health Consensus Development Conference Statement: Phenylketonuria: Screening and management, October 16-18, 2000", Pediatrics, 108:972-982 (2001)

[22] Scriver CR, Kaufman S, Eisensmith RC, Woo SLC, The hyperphenylaninemias. In: Scriver CR, Beaudet AL, Sly WS, Valle D, eds. Metabolic basis of inherited disease. Vol 1. 17th ed. New York, NY: McGraw-Hill;:1015–107 (1995)
[23] Gourovitch ML, Craft S, Dowton SB, Ambrose P, Sparta S., "Interhemispheric transfer in children with early-treated phenylketonuria", J Clin Exp Neuropsychol, 16(3):393-404 (1994)
[24] Banich MT, Passarotti AM, White DA, Nortz MJ, Steiner RD, "Interhemispheric interaction during childhood: II. Children with early-treated phenylketonuria", Dev Neuropsychol, 18(1):53-71(2000)
[25] Christ, SE, Huijbregts, SCJ, de Sonneville, LMJ, "White, DA Executive function in early-treated phenylketonuria: Profile and underlying mechanisms", Molecular Genetics & Metabolism. (in press).
[26] White, DA, Connor, LT, Nardos, B, Shimony, JS, Archer, R, Snyder, AZ, Moinuddin, A, Grange, DK, Steiner, RD, McKinstry, RC, "Age-related decline in the microstructural integrity of white matter in children with early- and continuously-treated PKU: A DTI study of the corpus callosum", Molecular Genetics & Metabolism. (in press).